Gold-Thiolate Clusters: A Relativistic Density Functional Study of the Model Species $Au_{13}(SR)_n$, R = H, CH_3, n = 4, 6, 8

Alexander Genest, Sven Krüger, Alexei B. Gordienko [a], and Notker Rösch

Department Chemie, Technische Universität München, D-85747 Garching, Germany
[a] *Permanent address:* Department of Physics, Kemerovo State University, 650043 Kemerovo, Russian Federation

Reprint requests to Prof. Dr. N. Rösch. E-mail: roesch@ch.tum.de

Z. Naturforsch. **59b,** 1585 – 1599 (2004); received September 15, 2004

Dedicated to Professor Hubert Schmidbaur on the occasion of his 70th birthday

The binding of sulfanyl and alkylsulfanyl model ligands to gold clusters was studied for the case of $Au_{13}(SR)_n$ with R = H, CH_3 and $n = 4$, 6, 8. Accurate all-electron electronic structure calculations and geometry optimizations of these gold-thiolate clusters have been performed with a scalar relativistic Kohn-Sham procedure as implemented in the density functional program PARAGAUSS. In all structures obtained, bridge coordination was preferred for both types of ligands; no higher coordinated sites where occupied. While in many cases ligand decoration did not change the overall structure of the Au_{13} core, also more open structures with Au-Au distances elongated beyond the bulk value have been obtained. The effects due to increasing ligand decoration were small: a small decrease of the binding energy per ligand does not exclude higher ligand coverages. The differences between the model ligands SH and SCH_3 were consistent in all cases considered: SCH_3 exhibits weaker binding and a slightly smaller charge separation between cluster core and ligand shell, which amounts up to about 1.5 *e* for 8 ligands. Overall, the Au_{13} core of the clusters was found to be quite flexible. This can be rationalized by the fact that the calculated binding energy per ligand is comparable or even exceeds the binding energy per atom in Au_{13}.

Key words: Gold Clusters, Gold-Thiolate Bonding, Relativistic Density Functional Calculations

Introduction

Since their first synthesis [1], gold clusters stabilized by alkylsulfanyl ligands SR attracted increasing interest as building blocks for nanostructures. Their versatile chemistry allows easy functionalization and modification with potential applications in various areas of technological importance [2, 3]. With their tunable properties, such clusters are useful to contact biomolecules in a well defined way [3 – 5]. Assembled in ordered arrays, gold-thiolate clusters are expected to form interesting quantum dot materials for nanoelectronics [6, 7]. However, despite considerable experimental effort, there are still many questions open with respect to the fundamental properties of thiolate-stabilized gold clusters [2]. Even seemingly simple geometric aspects like the coordination type of the sulfur head group at the gold cluster are still controversially discussed [8 – 11].

There have been several theoretical efforts to contribute to the understanding of structure, bonding, and electronic characteristics of this class of cluster compounds. Some density functional (DF) calculations, using models of one [8] or two [9] sulfanyl ligands interacting with a gold cluster, aimed at determining the binding site and examined the electronic structure with respect to thiolates as electronic linkers. For methylsulfanyl SMe on Au_{13}, a threefold hollow position has been calculated [8], whereas for 2 SMe ligands a bridge coordination was determined [9]. The interaction of an alkylsulfanyl with small gold species of a few atoms was also studied [12 – 14] with DF approaches. Thiolate covered gold clusters with more than hundred Au atoms and thiolates with long alkane substituents have been treated with simplified methods [10], where different coordination sites have been found to be occupied on a single cluster. For the cluster $Au_{38}(SMe)_{24}$, assuming a truncated cuboctahedral structure with ligands attached to bridge sites, in a detailed study using an accurate pseudopotential plane-wave density functional approach [11], a bridge coordination was determined for the ligands. There is

computational evidence based on DF calculations that disordered isomers are preferred for bare gold clusters [15 – 17]; also for thiolate covered species, disordered structures of the metal core have been proposed to be more stable than symmetric clusters [18]. The computational studies of gold-thiolate clusters thus far focuses on selected structures only, and quantitative (absolute) results on bond lengths and especially ligand binding energies are rare.

The coordination site of thiolates on Au clusters and surfaces is also the subject of intense debate: While early experiments suggest a threefold coordination [19], recent photoelectron diffraction [20] as well as normal incidence X-ray standing wave results [21] propose on-top adsorption, for SMe as well as for sulfanyls with longer alkyl chains, on the Au(111) surface. A high resolution electron energy loss study, on the other hand, has been interpreted to show multiple adsorption sites to be occupied, and even changes with the alkyl chain length [22]. Also DF calculations lead to different conclusions about the binding site of short chain alkyl thiolates [23]. Only some representative examples shall be mentioned. A Car-Parinello molecular dynamics study found threefold coordination of SMe on Au(111) [24], whereas in a cluster model with periodic boundary conditions [25] as well as in a supercell model calculation [26] the bridge site has been found to be favorable for the same system, as well as for thiolates with longer substituents [26].

A remark seems to be in order regarding the nomenclature used in this work. While $Au_m(SR)_n$ clusters are often referred to as "gold-thiols", we prefer the designation "gold-thiolate clusters" although we do not want to imply a complete charge separation where ligands carry a full negative charge, SR^-. Furthermore, we will use the term alkylsulfanyl when we want to emphasize the radical character of SR ligands; it will be clear from the context, when "sulfanyl" refers in a generic fashion both to SH and SR moieties.

The goal of the present work is to contribute to the understanding of thiolate-covered gold clusters by means of a model study applying an accurate all-electron relativistic density functional approach. The small cluster model Au_{13} has been chosen as it allowed us to inspect a larger number of structures of the ligand shell. Sulfanyl SH as a model ligand as well as methylsulfanyl SMe = SCH_3 as the smallest thiol-derived radicals have been considered. To gain insight in the effect of ligand coverage, 4, 6, and 8 ligands have been attached to the model cluster at various coordination sites. In this way, we present the first systematic computational study on how properties of gold thiolate clusters vary with structure, ligand type, and coverage. In the following, we first describe computational details and introduce the model compounds chosen. Then we present and discuss the results calculated for structural, energetic, and electronic properties.

Computational Details

All-electron calculations have been carried out with the LCGTO-FF-DF method [27] (linear combination of Gaussian-type orbitals fitting functions density functional) as implemented in the parallel program PARAGAUSS [28, 29]. Scalar relativistic effects have been taken into account with the Douglas-Kroll-Hess (DKH) approach to the Kohn-Sham problem [30 – 32].

All calculations were carried out in spin-unrestricted fashion since Au_{13} as well as $Au_{13}(SR)_n$ (R = H, CH_3; $n = 4, 6, 8$) contain an odd number of electrons. The structures were optimized with the local density approximation (LDA) in the parameterization proposed by Vosko, Wilk, and Nusair (VWN) [33]. Then at equilibrium geometries, binding energies were determined with a gradient-corrected exchange-correlation functional (generalized gradient approximation, GGA), using the functional proposed by Becke and Perdew (BP) [34, 35]. This "single point" strategy provides sufficiently accurate binding energies in a very efficient manner; results of full GGA optimizations are underestimated by less than 5 kJ/mol [36]. LDA often yields more accurate results for bond distances whereas GGA functionals provide more reliable energetic parameters [37 – 39]. Vertical ionization potentials (IPs) and electron affinities (EAs) as well as other features of the electronic structure have been determined at the self-consistent LDA level. For the numerical integration of the exchange-correlation contributions, a superposition of atom centered spherical grids [40] was chosen, using an angular grid that is locally accurate up to angular momentum L = 19 [41]. This corresponds to about 15620, 11990, 8580 and 6710 grid points for Au, S, C, and H, respectively.

The Kohn-Sham orbitals were represented by flexible Gaussian-type basis sets [42], contracted in a generalized fashion. For Au, a (19s, 15p, 10d, 6f) basis set was contracted to [9s, 8p, 5d, 2f]. For S as well as C the basis sets (12s, 9p, 2d) and (9s, 5p, 1d) were contracted to [6s, 5p, 2d] and [5s, 4p, 1d], respectively. For H, the contraction (6s,1p) $\rightarrow$ [4s, 1p] was chosen.

Table 1. Structural and electronic properties of the Au_{13} cluster model for various symmetry constraints. Average nearest-neighbor distance ⟨d⟩ as well as Au-Au bond lengths C-A and C-E in Å, binding energy BE per atom in kJ/mol, ionization potential IP and electron affinity EA in eV. The configuration is characterized by the four highest-lying orbitals, which are listed in the order of spin averaged orbital energies. For the atom labels C, A, and E, see Fig. 1.

Cluster	Distances			A-C-A	BE	IP	EA	Configuration
	⟨d⟩	C-A	C-E					
O_h	2.730	2.730	2.730	60.0	193.6	7.17	3.77	$a_{1u}{}^2t_{2g}{}^5$
D_{4h}	2.731	2.764	2.664	59.1	194.1	7.21	3.66	$a_{1u}{}^2e_g{}^4\ b_{2g}{}^1$
D_{3d}	2.733	2.740	2.725	60.7	194.4	7.19	3.74	$a_{1u}{}^2e_g{}^4\ a_{1g}{}^1$
D_{2h}	2.731	2.764	2.664	59.1	194.1	7.12	3.66	$a_{1u}{}^2b_{3g}{}^2\ b_{2g}{}^2b_{1g}{}^1$

In the LCGTO-FF-DF method, the classical Coulomb contribution to the electron-electron interaction is evaluated by representing the electronic charge density with an auxiliary Gaussian basis set of "fitting functions" [27]. The functions of s- and r^2-type of this auxiliary basis set were constructed in a standard fashion by scaling the exponents of the orbital basis sets [27]; furthermore, the auxiliary basis was supplemented by p- and d-type "polarization functions". Thus, for Au, the auxiliary charge density basis set was of the size (19s, $7r^2$, 5p, 5d); the auxiliary basis sets for S, C, and H were (12s, $9r^2$, 5p, 5d), (9s, $5r^2$, 5p, 5d), and (6s, $1r^2$, 5p), respectively. The p- and d-type "polarization exponents" were chosen as geometric series with factors of 2.5, starting at 0.1 and 0.2 au, respectively.

In all calculations, the elements of the density matrix were converged to at least 10^{-8} au. Geometries were considered to be converged when the maximum component of the energy gradient and the optimization step had dropped below 10^{-5} au.

Models

The cuboctahedral model system Au_{13} is the smallest cluster with a bulk like 12-fold coordinated central atom. This model was selected due to its small size, high symmetry, and the large number of symmetry subgroups, allowing an efficient treatment of different ligand coordinations and orientations for a varying number of ligands. To generate reference structures and energies, we optimized Au_{13} in O_h symmetry as well as by applying symmetry constraints according to the subgroups D_{4h}, D_{3d}, and D_{2h} (Table 1). Also these structures of lower symmetry have to be regarded as models because there is evidence that the ground state structure of Au_{13} is amorphous [15–17]. On the other hand, ordered structures have been found experimentally for the metal cores of larger Au cluster species [43–45].

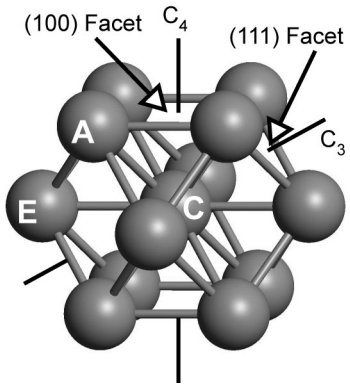

Fig. 1. Cuboctahedral cluster Au_{13}: Symmetry axes C_4 and C_3, facets and labels of atoms (C = central, E = equatorial, and A = axial).

Fig. 1 shows the cluster Au_{13} in cuboctahedral symmetry, featuring pertinent symmetry elements as well as labels of facets and atoms. In the following the central atom will be referred to by the label C. Au atoms in the surface are distinguished by axial (A) and equatorial (E) coordination with respect to the main symmetry axis of the structure under consideration. In D_{4h} and D_{2h} symmetry, the cluster is terminated at top and bottom by one of its six (100) facets, each composed of four axial gold atoms. Four equatorial atoms form a square in the horizontal symmetry plane. In D_{3d} symmetry, (111) facets terminate the cluster at top and bottom, each formed by three axial atoms. The middle layer of the cluster now consists of the central atom, surrounded by a hexagon of six equatorial atoms (see Fig. 1).

We examined various ligand coordination sites of the cluster model Au_{13} by attaching 4, 6, and 8 SR ligands according to D_{2h}, D_{3d}, and D_{4h} symmetry, respectively (Fig. 2). When the structures are optimized with respect to all degrees of freedom compatible with these symmetry constraints, ligands can move to a certain extent between different high-symmetry sites (Fig. 3);

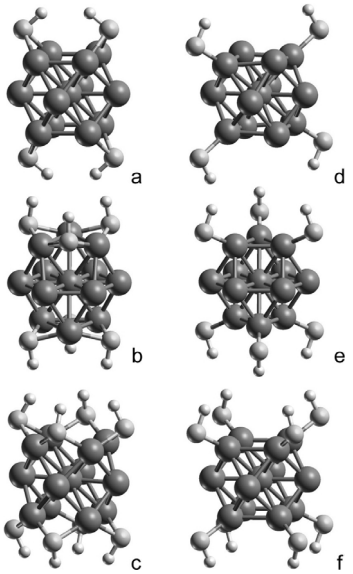

Fig. 2. Four, six, and eight SH ligands on Au_{13} for axial ligand orientation, with D_{2h}, D_{3d}, and D_{4h} symmetry constraints, respectively. a), b), and c): bridge coordination (b ax); e), f), and g): top coordination (t ax).

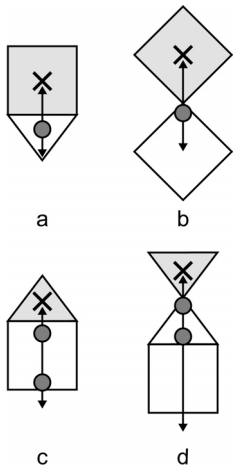

Fig. 3. Determination of the sulfur sites in symmetry-restricted geometry optimizations of thiolate-ligated Au_{13} clusters. The freedom of movement from a starting site (marked as grey circle) is indicated by arrows; crosses mark the main symmetry axes on the "top" facets (shaded in grey). a) D_{nh}, bridge–hollow site; b) D_{nh}, top site; c) D_{3d}, bridge–fourfold site; d) D_{3d}, top–threefold site.

this allows one to scan various sites without having to resort to a computationally demanding lower symmetry. If eight ligands are treated in D_{4h} symmetry, ligands are attached singly coordinated (top) to Au atoms of the top and bottom (100) facets or between these

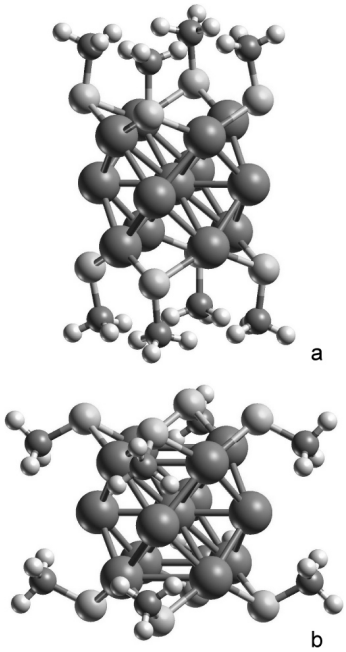

Fig. 4. Au_{13} clusters with SMe ligands in bridge position and axial (a) as well as equatorial (b) orientation.

atoms in bridge coordination. Bridge coordination allows the ligands to move closer to the horizontal symmetry plane of the cluster and thus to the center of the triangular (111) facet on the cluster surface representing a threefold coordination for the S head atom (Fig. 3a). On the other hand, top coordination permits only a slight movement of the ligand in the vicinity of that site (Fig. 3b). In the case of D_{2h} symmetry, the various surface sites are accessible in the same way, except that now only two instead of four ligands are placed near the top and bottom facets of the cluster, respectively.

As indicated by the arrows in Figs. 3c and 3d, D_{3d} symmetry provides more freedom for positioning the six ligands treated in that case because the horizontal symmetry plane is missing. Therefore, during geometry optimization, a set of ligands can, in principle, move from the top face of the cluster to the bottom face and *vice versa*. In the symmetries D_{4h} and D_{2h}, this is not possible as symmetry equivalent ligands would meet each other. As illustrated by Fig. 3c ligands at bridge positions of top and bottom facets of Au_{13}, arranged in a starting configuration of D_{3d} symmetry, may also reach fourfold coordinated sites. In that symmetry, adjacent threefold sites as well as bridge positions different from those of the top or bot-

tom facets are accessible when starting from on-top coordination at the top/bottom (111) facets (Fig. 3d). By moving even further, the ligands may reach again fourfold sites which are equivalent to those close to the starting bridge configuration (Fig. 3d). To scan various ligand coordination modes in D_{3d} symmetry, we chose several starting positions, as indicated by the grey circles in Figs. 3c and d. Overall, our series of models covers top, bridge, threefold, and, where applicable, also fourfold coordination of SR ligands at coverage values S:Au between 0.3 and 0.6, which corresponds to the range in experimental determinations for larger clusters [2, 46, 47].

Besides inspection of various coordination sites, also different ligand orientations have been considered. In the starting geometries, the S-R bond of the ligands was oriented either in the direction of the main axis (axial orientation) or about perpendicular to it (equatorial orientation). Examples of optimized results for axial and equatorial orientations are given in Fig. 4.

Results and Discussion

In the following we will discuss our computational results starting with the bare Au_{13} cluster. Then we present the results for ligated cluster models. Depending on the starting configuration, a variety of different structures has been obtained, even though the flexibility of our models was constrained by symmetry. We start with "regular structures" where ligand coordination does not affect the Au-Au coordination in a significant way, implying only a moderate distortion of the internal structure of the cluster core. Most of these structures were obtained when ligands were attached to top and bottom facets of the Au_{13} cluster. Subsequently, we will discuss structures where metal bonds are considerably elongated, leading to strongly deformed cluster cores, to which we refer as "irregular structures". Structures of this type are preferentially found in D_{3d} symmetry when ligands where arranged around the central layer of the metal cluster. As will be discussed below, the flexibility of the Au_{13} core allows quite a variety of ligand arrangements on the cluster surface. Therefore, the set of structures obtained in our study cannot be regarded as exhaustive.

Au_{13}

For $Au_{13}(O_h)$ we calculated a bond length of 2.73 Å and a binding energy per atom of 194 kJ/mol (Table 1). Because the highest occupied molecular orbital (HOMO) in O_h symmetry is not completely filled ($t_{2g}{}^5$), a Jahn-Teller distortion results when the symmetry is reduced. However, symmetry lowering entailed only small changes in shape and binding energy per metal atom (Table 1). The average Au-Au distance remained essentially constant, with increases of at most 0.003 Å. The binding energy per atom increased by up to 0.8 kJ/mol (D_{3d}, Table 1), which leads to an overall stabilization of the cluster by 10 kJ/mol only. In D_{4h} the bond length C-A between central and axial Au atoms (Fig. 1) increased by 0.03 Å, while the central-to-equatorial bond C-E decreased by 0.07 Å relative to the octahedral structure. This results in a slight cylindrical distortion of the cluster. As the electronic configuration in D_{4h} exhibits a singly occupied b_{2g} HOMO, no Jahn-Teller distortion is possible by further symmetry reduction. Thus, the same structure as for D_{4h} is obtained in D_{2h} symmetry. In case of a symmetry reduction from O_h to D_{3d}, we observed even smaller effects on the structure than for D_{4h}. Both pertinent bond lengths C-A and C-E changed by less than 0.01 Å, thus the cluster preserves its overall spherical shape. In all cases, angles changed less than one degree. IPs and EAs changed at most 0.1 eV when the symmetry constraint was reduced (Table 1). Whereas identical in all other properties, the D_{4h} and D_{2h} structures showed a small difference in the IP. In the case of D_{4h} symmetry, the fully occupied e_g set is ionized, whereas in D_{2h} symmetry a singly occupied b_{2g} spin orbital is emptied. Thus, the final states of the cation differ in these two symmetries.

By means of many-body potentials, truncated octahedral and decahedral structures have been determined to be most stable for bare gold clusters with diameters of a few nm [44, 48]. For Au_{13} and larger symmetric clusters, several calculations found an icosahedral structure to be less stable than a cuboctahedral one [17, 49, 50], the latter thus being the most stable high-symmetry structure of Au_{13}. Our results for the Au-Au bond length of $Au_{13}(O_h)$, 2.73 Å, is very similar to that of a previous study, using the same computational method, but a less flexible auxiliary basis set [17]. In that work, a bond length of 2.74 Å had been determined at the LDA level, whereas the corresponding GGA(BP) calculation yielded 2.83 Å, in rough agreement with a recent pseudopotential PW91 result of 2.78 Å [17]. For this bond distance, also larger values of 2.9 Å and beyond have been obtained by hybrid [8] and GGA functional [51] DF calculations with pseudopotentials. As these distances exceed the bulk

Table 2. Ligand-related characteristics of $Au_{13}(SR)_n$, R = H, Me: nearest (S-Au) and next nearest (S-Au2) bond lengths between S and Au in Å, bonding angles in degree, and binding energies BE per ligand in kJ/mol. The structures are labeled by symmetry, coordination site (b = bridge, t = top), and ligand orientation (ax = axial, eq = equatorial).

Structure		*n*	S-Au		S-Au2		S-R		Au-S-R		BE	
			H	Me	H	Me	H	Me	H	Me	H	Me
D_{2h}	b ax	4	2.396	2.373	3.529	3.182	1.366	1.815	96.1	102.1	256	232
	b eq		2.394	2.366	3.567	3.480	1.366	1.815	98.1	107.4	258	238
	t ax		2.270	2.266	4.352	4.338	1.364	1.812	95.8	105.1	220	199
D_{3d}	b ax	6	2.404	2.396	3.290	3.245	1.370	1.836	97.7	105.5	244	218
	b eq		2.417	2.394	3.509	3.607	1.370	1.812	96.9	112.3	242	220
	t ax		2.278	2.275	3.766	3.772	1.365	1.811	94.8	104.3	205	184
	t eq		2.264	2.260	4.510	3.833	1.365	1.817	95.3	113.1	209	174
D_{4h}	b ax	8	2.416	2.406	3.058	2.979	1.369	1.830	97.7	108.6	244	215
	b eq		2.434	2.425	3.163	3.197	1.366	1.825	97.7	107.0	242	211
	t ax		2.266	2.267	4.123	4.152	1.365	1.812	94.5	103.1	215	194
	t eq		2.263	2.261	4.106	4.171	1.365	1.812	96.6	106.2	216	191

nearest-neighbor value for gold of 2.88 Å [52], they are not regarded as trustworthy because average interatomic distances decrease with decreasing cluster size [49, 50, 53].

To the best of our knowledge, there are no recent values for the absolute binding energy of Au_{13} in the literature. By means of empirical and first principles calculations, stable disordered isomers of small gold clusters have been identified [15 – 17]. In GGA calculations on Au_{13}, the most stable amorphous species have been found to be by about 135 kJ/mol more stable than the octahedral structure [16,17]. Because several almost degenerate disordered structures have been identified, there is some evidence that small gold clusters are quite flexible, changing dynamically between various low lying minima on the potential energy surface. Taking these uncertainties about the structure into account, Au_{13} with a distorted cuboctahedral structure, as applied here, should be regarded as a reasonable model system to inspect various aspects of the interaction of gold clusters with alkylsulfanyl ligands.

Regular structures

Structure and stability

In Table 2, pertinent geometric parameters related to the coordination of SR ligands to Au_{13} are collected for R = H, Me and increasing ligand coverage from 4 to 8. Also axial and equatorial types of ligand orientation, *i. e.* roughly parallel and perpendicular to the main axis, are distinguished. For D_{2h} symmetry and top coordination, only one type of ligand orientation (axial) has been listed because it is equivalent to equatorial orientation, the latter being "axial" with respect to one of the horizontal C_2 axes.

In all cases considered, the low coordinated sites, on-top and bridge, are favored by SH and SMe ligands (Figs 2 and 4). Comparing S-Au and next-nearest distances S-Au2 (Table 2), one notes that secondary contacts S-Au2 are considerably longer than the contacts S-Au involved in top or bridge coordination. The shortest S-Au2 distances are obtained for eight ligands in bridge coordination and axial orientation; they amount to 3.06 Å for SH and 2.98 Å for SMe and are by about 0.6 Å longer than S-Au bonds. For this coordination weak steric repulsion among the ligands arranged around the top (100) facet of the cluster leads to the largest displacement of S centers in the direction to a threefold site. Still, the ligands are far from a threefold coordination, as seen in Figs 2 and 4. This rationalization is corroborated by comparing the same cluster species, but with equatorial ligand orientation where steric crowding around the top (100) facet is avoided. This latter situation results in a shift of the ligands towards the bridge site, increasing the S-Au2 distance by ~ 0.1 Å.

Simplified bonding arguments also result in a preference for low coordinated sites. Neutral species $Au_{13}(SR)_n$ can be partitioned into a neutral metal cluster and a set of sulfanyl radicals. The sulfur center of the ligands carries a singly occupied p orbital as well as a p lone pair, besides the low lying 3s orbital and the third p orbital involved in bonding to H or Me. On-top binding involves only the free valence, while bridge coordination also benefits from a dative bond *via* the S 3p lone pair. No further orbitals are available for bonding without strong rehybridization. A Mulliken analysis of the orbitals reveals that the situation is more involved. The low lying 3s orbitals of S also participate in the bonding to H or Me in the ligands and the

Table 3. Cluster-core related characteristics of $Au_{13}(SR)_n$, R = H, Me: average Au-Au coordination numbers c and distances ⟨d⟩ as well as selected Au-Au bond lengths and angles. Structures are labeled by symmetry, coordination site (b = bridge, t = top), and ligand orientation (ax = axial, eq = equatorial). Bond lengths in Å and angles in degree. For the atom labels C, A, and E, see Fig. 1.

Structure		*n*	c		⟨d⟩		C-A		C-E		A-C-A	
			H	Me	H	Me	H	Me	H	Me	H	Me
D_{2h}	b ax	4	5.54	5.54	2.766	2.771	2.797	2.811	2.723	2.657	58.5	56.4
	b eq		5.54	5.54	2.766	2.768	2.793	2.778	2.724	2.735	58.7	58.0
	t ax		5.54	5.54	2.742	2.742	2.710	2.715	2.671	2.766	60.1	60.1
D_{3d}	b ax	6	5.54	5.54	2.827	2.830	2.938	2.944	2.710	2.709	63.0	62.6
	b eq		4.62	4.62	2.816	2.826	2.895	2.909	2.735	2.739	65.0	65.6
	t ax		5.54	5.54	2.738	2.738	2.752	2.748	2.725	2.728	59.7	59.8
	t eq		5.54	5.54	2.759	2.735	2.808	2.728	2.702	2.742	63.1	60.4
D_{4h}	b ax		4.31	4.31	2.845	2.843	2.935	2.930	2.646	2.649	65.1	64.4
	b eq	8	4.31	5.54	2.837	2.824	2.930	2.915	2.629	2.623	64.5	63.2
	t ax		5.54	5.54	2.744	2.744	2.749	2.755	2.731	2.721	61.0	60.9
	t eq		5.54	5.54	2.743	2.744	2.758	2.756	2.717	2.720	60.8	61.1

preference of low coordinated sites may be due to the different orientations of S 3p lone pairs. Also for gold-phosphin thiolate complexes, two- and three-fold coordination of sulfur is most common [54], which corresponds to top and bridge coordination at the cluster surface, respectively.

The binding energies compiled in Table 2 clearly imply a preference for bridge sites. While top coordinated ligands are bound by 175 to 220 kJ/mol, bridge coordination of ligands entails a stabilization by 210 to 260 kJ/mol. For clusters with the same number of ligands, bridge coordination is calculated to be favored by 20 to 40 kJ/mol per ligand, irrespective of the ligand orientation. SMe ligands are calculated to be bound less strongly than SH ligands by 20 to 30 kJ/mol (Table 2). Surprisingly, ligand coverage does not affect the binding energy per ligand in a major fashion. For both types of ligands examined, the strongest bonds are calculated if only four ligands are attached in bridge coordination. Increasing the number of ligands to six and eight decreases the binding energy per ligand by less than 20 kJ/mol, *i.e.* by about 10% only. In case of bridging SH ligands, no difference is seen between six and eight ligands; eight SMe ligands are even slightly stronger bound than six. Similar but even weaker trends were obtained for singly coordinated ligands. The result that four ligands are stronger bound than six or eight, but no notable difference is found between clusters with six and eight ligands, can be rationalized by appealing to bonding competition at the metal centers forming the bonding sites. For four ligands in on-top coordination, the neighboring Au centers of the site do not carry ligands, whereas two of the neighboring Au atoms are ligated when six or eight ligands are present. For four bridge-bonded ligands, each Au atoms is involved only in a single bridge site, whereas for six and eight ligands, each of these Au atoms is involved in two bridge sites. The binding energy per ligand of the two ligand orientations inspected deviates at most by 10 kJ/mol (Table 2). Thus, steric interactions are not of strong importance for the small ligands considered in this study. In similar model calculations on $Cu_{13}(SEt)_8$ [55], using a hybrid force field and density functional approach (QM/MM), it was found that steric interactions among the ethylthiolate ligands become noticeable.

Top and bridge coordinated thiolates also result in clearly different structural characteristics. Parameters with regard to the ligand coordination are compiled in Table 2, while pertinent data for the Au_{13} cluster core are collected in Table 3. The S-Au bond length varies between 2.26 and 2.29 Å for top sites, whereas 2.37 to 2.43 Å are obtained for bridge coordinated ligands. Thus, the bonds at top sites are ~ 0.1 Å shorter than the two bonds to the Au centers that form a bridge site. The two distance ranges are hardly different for the two types of ligands considered: 2.26 – 2.29 Å for top and 2.39 – 2.43 Å for bridging SH; 2.26 – 2.29 Å for top and 2.37 – 2.43 for bridging SMe. A more detailed inspection of the results uncovers only weak differences. With regard to coverage, no clear trend of bond lengths is identified for top coordination. For SH as well as SMe at bridge positions, the Au-S bond lengths increase slightly with coverage, in line with the decrease of the binding energy (see above). On going from four to six ligands, the Au-S bonds elongate by 0.01 to 0.03 Å for both types of ligands, independent of orientation; yet again the same elongation is calculated when the coverage increases further to eight ligands (Table 2). This finding is in line with the concept

of bonding competition; this argument also nicely explains why no such trend is found in case of on-top coordination where bond competition is absent. Comparing SH and SMe ligands, the latter show a trend to shorter S-Au bonds by as much as 0.02 Å, although for SMe a tendency to lower binding energies is calculated (see above). This finding can be traced back to the strength of the intra-ligand bond which is weaker in S-Me than in S-H.

In all cases, bond angles Au-S-R are larger than the corresponding angles H-S-R in the free thiols, 92° for HSH and 98° for HSMe. For SH, this increase amounts to 3–6°, but it may be up to 15° for SMe. The intra-ligand bond length S-H of SH is always calculated somewhat longer than in HSH, where it is 1.359 Å. This bond length hardly varies, at most by 0.006 Å. A larger variation is obtained for the S-C bond in SMe, which also is always longer than the value of 1.811 Å in HSMe. Here, we found an almost regular trend of longer bonds, up to 1.84 Å, for the stronger bound bridge coordination whereas in top coordination 1.82 Å is not exceeded.

Because the average binding energy per Au atom in Au_{13}, 194 kJ/mol (Table 1), is comparable to the weakest ligand binding energies, one expects that ligand association to the cluster significantly affects the geometry of the cluster core. Nevertheless, inspection of average Au-Au distances of thiolate covered clusters (Table 3) shows only a moderate elongation by 0.01–0.05 Å in most cases. Stronger ligand effects occur for six and eight bridging ligands where the average Au-Au distance is enlarged by about 0.1 Å to 2.83 Å. Ligand coordination to a bridge site always entails a stronger effect on average Au-Au distance of the cluster than top coordination, in line with the higher binding energy. On the other hand, the small difference between binding energies for top and bridge coordination (Table 3) is probably not the primary reason for the stronger effect of bridging coordination on the structure of the metal core: once again, bond competition seems to be more important. Also the angles between the surface and central atoms stay close to the ideal value of 60° of a cuboctahedron. As an example, we list the angles A-C-A in Table 3. They vary at most 5°, but for the majority of species this angle deviates less then 3° from the reference value. In agreement with the stronger interaction of bridged ligands, larger deviations from 60° are obtained for bridging than for top coordination (Table 3). In most cases, opening of the A-C-A angle by some degrees is accompanied by an oblate distortion of the quasi-spherical cluster shape; only in the case of four bridging ligands, the angle A-C-A decreases slightly (prolate distortion).

Close inspection of different metal-metal bonds reveals that individual distances vary considerably although the cluster core on average expands only moderately (Table 3): For the C-E bonds, values between 2.62 and 2.77 Å were calculated, and the C-A bond scattered from 2.70 to 2.94 Å. Compared to the Au-Au bond length of the bare cluster (2.73 Å) and the experimental bulk inter-atomic distance of gold of 2.88 Å [52], some of the Au-Au distances in the thiolate-ligated compounds are rather long. In Table 3 we list the (average) gold-gold coordination numbers c as indicator for the presence of especially long Au-Au bonds; to determine the coordination number, we used 3.1 Å as somewhat arbitrary upper value for "bonding" interactions. As discussed for the average Au-Au distance, species with six and eight bridging ligands show a decrease in coordination below the value of 5.5 for Au_{13}. Summarizing the geometric results for regular structures, we note that the metal core reacts in a rather flexible way to ligand coordination, but essentially preserves its overall structure and the inter-metal coordination.

Recently, rather small thiolate-stabilized gold clusters have been synthesized [56, 57]. Yet, to the best of our knowledge, there is no experimental information regarding ligand binding energies and structural parameters of such thiolate-covered gold clusters. For a few clusters (Au_{28}, Au_{38}), disordered structures, with the sulfur atoms of the thiolate ligands incorporated in the strongly distorted surface layer of the gold cluster, have been computationally determined to be more stable than ordered structures [15,18,58]; unfortunately, no definite information about binding energies and coordination sites has been published for these species; inspecting sketches of these structures [58], one notes that different sites are occupied. Taking into account the rather small energy variation between top and bridge coordination calculated in this work, it seems plausible that different coordination modes occur on the facets of a highly disordered cluster surface.

The computational study most similar in spirit to the present model investigation also used a DF-LDA approach, but a rather different computational technology based on pseudopotentials (*e.g.*, explicitly accounting only for 11 valence electrons of Au) and a plane-wave representation of the Kohn-Sham orbitals [11]. With this methodology, the structure of $Au_{38}(SMe)_{24}$

was optimized without symmetry constraints. In agreement with our findings, a structure was obtained where methylsulfanyls were coordinated at bridge sites of the (111) facets of the truncated cuboctahedral cluster core. The Au-S bond lengths of 2.52 Å are longer than those calculated here for $Au_{13}(SMe)_8$, $\sim$ 2.4 Å; also, the Au-S-C angles of 126° exceeded those obtained in our work, $\sim$ 110° (Table 2). Because the ligand coverage of the Au clusters was similar in both studies [0.75 ligands per surface Au atom in $Au_{38}(SMe)_{24}$ and 0.67 for $Au_{13}(SMe)_8$] one can most likely rule out steric differences as source of these discrepancies, but calculated binding energies provide a hint. The GGA value for the binding energy per gold atom in Au_{38} was calculated slightly larger, 203 kJ/mol [11], than the GGA value of our study (194 kJ/mol, Table 1). Note also that the binding energy per metal atom is known to increase with cluster size size [49, 50]. On the other hand, the GGA ligand binding energy in $Au_{38}(SMe)_{24}$ of 134 kJ/mol [11] is considerably smaller than the present values (Table 2) and also results of other computational studies [9] (see below). Thus, in the study of Ref. 11, bond competition at metal atoms of the cluster surface is different due to a severe underestimation of Au-S bonds compared to Au-Au bonds; this systematic difference rationalizes the observed structural discrepancies.

In a recent DF-GGA study of $Au_{38}(SMe)_2$ [9], also employing pseudopotentials, the thiolate ligands have been found to prefer bridge sites between two (111) facets. There, considerably shorter Au-S bonds of 2.46 Å and a ligand binding energy of 209 kJ/mol have been determined. The bond strength of the thiolates seems again underestimated, especially if one takes into account the low coverage. The Au-S bonds were calculated longer than in our case for $Au_{13}(SMe)_4$ (Table 2); this may be due to fact that a GGA exchange-correlation functional has been used for the geometry optimization [37 – 39].

Another computational study, applying the hybrid exchange-correlation functional B3LYP together with a small-core pseudopotential for Au, examined the coordination of a single SMe ligand to the cluster Au_{13} [8]. At variance with the present work and results of other calculations discussed above, a threefold hollow site was determined as most stable; unfortunately, the value of the binding energy was not reported. The rather strong elongations of Au-Au bond lengths (up to 3.62 Å or 0.7 Å compared to Au_{13}! [8]) in that work seem questionable when contrasted with the smaller ligand effect on Au-Au distances determined in the present calculations for higher ligand coverages. Similar results were obtained for an phenylsulfanyl ligand SPh [8].

Table 4. Comparison of computational results of SR coordination in thiolate-ligated gold clusters $Au_m(SR)_n$. S-Au and S-C bond lengths in Å, binding energy BE per ligand in kJ/mol.

Method	R	m	*n*	Site[a]	S-Au	S-R	BE	Ref.[b]
AE-SR VWN/BP	H	13	4	b	2.39	1.37	256	pw
	H	13	6	b	2.40	1.37	244	pw
	H	13	8	b	2.42	1.37	244	pw
	CH_3	13	4	b	2.37	1.82	232	pw
	CH_3	13	6	b	2.40	1.84	218	pw
	CH_3	13	8	b	2.41	1.83	215	pw
ECP VWN/BP	CH_3	38	24	b	2.52	1.87	134	11
ECP PBE	CH_3	38	2	b	2.46	–	209	9
ECP B3LYP	CH_3	13	1	h	2.55	1.84	–	8

[a] Sites: bridge – b, threefold hollow – h; [b] references, pw = present work.

For very small gold particles with a few atoms only, a preference for low coordination of thiolate bonding has been proposed based on pseudopotential DF LDA [12] and hybrid functional calculations [13], but this result was questioned in a more extensive GGA DF pseudopotential plane wave calculation [14].

Also Au(111) surfaces with adsorbed thiolate overlayers have been examined computationally [9, 23, 25]. A comparison with our results seems worthwhile, but has to take into account two major differences with these surface model studies which aimed at self-assembled monolayers of thiolates on gold substrates. The structure of dense thiolate overlayers is not only determined by the ligand-substrate interaction, but also by ligand-ligand interaction, especially for thiolates with larger substituents. For the Au clusters studied here and in other computational investigations, ligand coverage as well as ligand size (SMe) prevents any sizeable ligand-ligand interaction; this is different when sulfanyls with longer alkyl chains are simulated [10, 55]. Secondly, the atoms of a Au(111) surface are coordinated by nine other metal atoms. This coordination of the substrate atoms is much larger than that (5 – 6) of atoms forming surface facets of small Au clusters (Table 3). Thus, one anticipates that sulfanyls interact weaker with an ideal Au(111) surface. DF GGA pseudopotential calculations yielded 178 kJ/mol for a boundary corrected cluster model and 163 kJ/mol in a periodic slab model for the favorite site close to a bridge [25]. These values are in agreement with an older estimate of 167 kJ/mol per adsorbat [59]. In agreement with a weaker bond, also Au-S distances

Table 5. Electronic structure of $Au_{13}(SR)_n$ clusters for R = H, Me, from LDA calculations: Mulliken charges q per ligand and of the cluster core Au_{13} in *e*, ionization potential IP, electron affinity EA, and energy ε_{HOMO} of the HOMO, in eV. Structures are labeled by symmetry, coordination site (b = bridge, t = top), and ligand orientation (ax = axial, eq = equatorial).

Structure		*n*	q(SR)		q(Au_{13})		IP		EA		ε_{HOMO}	
			H	Me	H	Me	H	Me	H	Me	H	Me
D_{2h}	b ax	4	−0.17	−0.09	0.70	0.36	6.94	6.21	3.60	3.23	−5.29	−4.88
	b eq		−0.15	−0.08	0.61	0.30	6.04	6.29	3.46	3.32	−5.15	−4.92
	t ax		−0.21	−0.15	0.86	0.61	6.88	6.50	3.77	3.51	−5.37	−5.06
D_{3d}	b ax	6	−0.19	−0.13	1.17	0.80	6.19	5.56	3.06	2.59	−4.63	−4.08
	b eq		−0.15	−0.11	0.91	0.69	6.60	6.13	3.45	3.14	−5.03	−4.64
	t ax		−0.18	−0.14	1.10	0.82	7.18	6.57	4.07	3.68	−5.70	−5.16
	t eq		−0.19	−0.11	1.13	0.66	7.11	6.65	3.99	3.81	−5.60	−5.24
D_{4h}	b ax	8	−0.22	−0.18	1.75	1.41	6.46	5.85	3.31	2.89	−4.93	−4.41
	b eq		−0.16	−0.10	1.25	0.82	6.47	5.81	3.33	2.87	−4.95	−4.38
	t ax		−0.18	−0.15	1.43	1.19	7.06	6.43	4.22	3.75	−5.65	−5.09
	t eq		−0.18	−0.15	1.47	1.16	7.06	6.48	4.22	3.80	−5.64	−5.13
$Au_{13}O_h$			0		0		7.17		3.77		−5.47	

of 2.56 Å (cluster) and 2.50 Å (slab model) [25] have been calculated longer than in the present work (Table 2).

Recent experiments [20, 21] on self-assembled monolayers favored on-top adsorption of thiolate ligands and hence re-opened the discussion of adsorption sites on gold surfaces. This latest turn of the case underlines the complexity of gold-thiolate adsorption systems and points toward the necessity of employing sophisticated substrate models for surfaces as well as for clusters that allow a flexible structural response to thiolate adsorption.

Electronic structure

To provide insight into the way how thiolate ligands affect the electronic structure of the model cluster Au_{13}, we discuss the density of states for $Au_{13}(SR)_8$, R = H, Me, with ligands at the most stable bridge positions (axial orientation). Fig. 5 shows various densities of states (DOS) which are based on valence orbital energy spectra subjected to a Gaussian level broadening with half width of 0.25 eV. The Fermi energy is determined by integrating the resulting DOS up to the total number of electrons of each cluster compound. Furthermore, partial densities of states, based on Au(sp), Au(d), and ligand contributions, have been derived from on a Mulliken population analysis of individual spin orbitals.

The cluster Au_{13} exhibits a 5d band (Fig. 5a) that is nearly 6 eV wide and features three major peaks. The valence 6sp DOS is very broad; it contributes to the total DOS in an appreciable fashion only near the Fermi energy, at ~ -5 eV and above. Attachment of sulfanyl ligands induces DOS contributions mainly between -6 and -12 eV as well as a smaller peak below the Fermi energy. Methylsulfanyl ligands give rise to strong peaks at -11.5 eV and -10.5 eV which mainly represent C-H bonding orbitals (Fig. 5c). As a result of ligand coordination, the Au 5d band broadens slightly, but the most important effect results near the Fermi energy. The DOS in that energy range is reduced and consists of small Au 5d and some ligand contributions, but a notable Au 6sp component is restricted to the unoccupied levels. Moreover, the Fermi level is shifted upward by about 0.2 eV due to SH (Fig. 5b) and 0.7 eV due to SMe (Fig. 5c) coordination. These

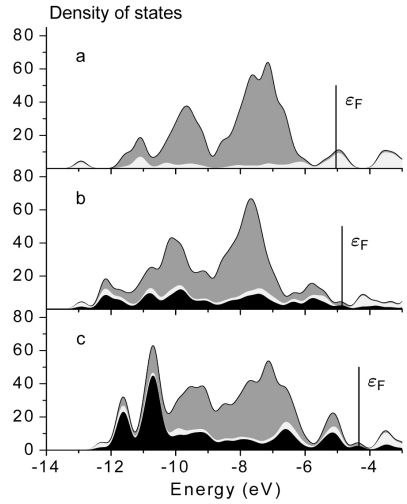

Fig. 5. Density of states (DOS) of an Au_{13} cluster in D_{4h} symmetry. Bare cluster (a), and clusters covered with eight SH (b) and SMe (c) ligands in axial orientation. Local DOS contributions from a Mulliken analysis. Ligands – dark shading, Au sp – white, Au d – grey shading. The Fermi level is indicated by a vertical line.

changes may be interpreted as propensity to reducing (or even quenching) the metal character of the core of the small Au_{13} cluster. The trends discussed are less pronounced for smaller numbers of ligands. For on-top coordination of eight ligands, the Au(sp) partial DOS is also considerably reduced, but a larger total DOS with mainly ligand and Au(d) contribution is obtained close to the Fermi level.

Electronic structure related parameters of all species considered are collected in Table 5. In line with the upward shift of the Fermi energy, the ionization potentials (IP) of all ligand covered clusters is calculated smaller (Table 5). Compared to the bare octahedral cluster Au_{13}, the IP is reduced by up to 0.7 eV for top coordinated thiolates and by up to 1.6 eV for ligands at bridge positions. The IPs show hardly any trend with variation of the ligand coverage. In almost all cases, SMe ligands reduce the IP more than the SH model ligands. This result may be rationalized with the stronger donor capability of a methyl group (compared to H) which results in an overall upward shift of the DOS (see above). EA values scatter around the value calculated for the free cluster Au_{13}, 3.77 eV. While on top coordination of ligands yields preferentially higher EAs, bridge coordinated ligands tend to lower the EA. EA values scatter over a smaller range than IP values; maximum deviations are 0.5 eV for top coordinated ligands and -1.2 eV for bridge coordinated ligands. As for the IP, EA values for SMe ligands are always smaller than those for the corresponding clusters with SH ligands. The present IP and EA values calculated for $Au_{13}(SR)_n$ are in very good agreement with results for $Au_{38}(SMe)_{24}$ [11]. For that larger cluster, an IP of 5.31 eV and an EA of 3.41 had been calculated at the LDA level. The trends discussed for IP and EA naturally correspond to the variation of the orbital energy ε_{HOMO} (Table 5). For the most stable configurations with ligands in bridge positions, the HOMO is raised to about -4.1 eV from -5.5 eV for the bare cluster Au_{13} (Table 5). This upward shift of the HOMO energy is smaller for ligands at on-top positions (up to -5.1); for six and eight SH ligands at on-top positions, the HOMO is even slightly stabilized, by up to -0.2 eV. Due to the donating capability of the methyl substituents, SMe ligands always induce a stronger upward shift of the HOMO than the SH model ligands.

The charge distribution in the ligated Au_{13} cluster has been monitored by means of a Mullikan population analysis. Charges of ligands and of the metal core of the cluster are collected in Table 5. As thiolate ligands (as a whole) are withdrawing electron charge density, the effective number of electrons on the gold cluster decreases with increasing number of ligands. For the largest coverage examined, about $1-1.5$ e are transferred to the ligand shell. On the other hand, the charge per ligand stays rather constant at -0.1 to -0.2 e, independent of coverage, at variance with the simple expectation that the charge per ligand decreases with increasing number of ligands. However, the tendency of the HOMO to shift to higher energies with increasing ligand decoration balances the effect of increasing charge withdrawal from the metal core, by facilitating transfer of electron density to the ligand. This leads to a more or less constant amount of charge drawn per ligand. The amount of charge separation estimated for $Au_{13}(SR)_n$ is in line with the findings in the previous calculation on $Au_{38}(SMe)_{24}$, where a charge transfer of ~ 2 e in total or about 0.08 e per ligand was estimated [11]. In the calculation on $Au_{13}SMe$ [8], the charge of the single thiolate ligand was determined at -0.11 e. Apparently, the amount of charge take-up by SMe ligands is fairly independent of the coverage; note, however, that a different computational method was used in that case. As for other properties discussed above, the stronger electron donating capability of methyl substituents compared to H is also apparent in the population analysis. Thus, irrespective of the coordination site, the negative charge per ligand is slightly lower for methylthiolate than for simple thiolate model ligands (SH), resulting in a smaller overall charge separation between metal core and ligand shell by ~ 0.25 e.

Irregular structures

In some of our calculations with D_{3d} symmetry constraints, we obtained structures with considerably elongated Au-Au distances where ligands were attached at bridge positions of the six-ring in the central metal

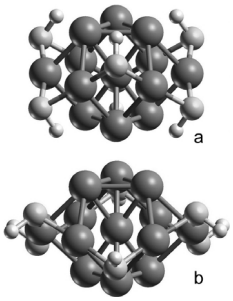

Fig. 6. Complex-like (irregular) structures of $Au_{13}(SH)_6$ with bridging SH in axial (b3 ax – a) and equatorial (b3 eq – b) orientation.

Table 6. Ligand-related characteristics of irregular structures of $Au_{13}(SR)_6$ in D_{3d} symmetry, R = H, Me: nearest (S-Au) and next nearest (S-Au2) bond lengths between S and Au in Å, bonding angles in degree, and binding energies BE per ligand in kJ/mol. Structures are labeled by coordination site (b3 = bridge toward threefold, b4 = bridge towards fourfold) and ligand orientation (ax = axial, eq = equatorial).

Structure	S-Au		S-Au2		S-R		Au-S-R		BE	
	H	Me	H	Me	H	Me	H	Me	H	Me
b3 ax	2.317	–	2.700	–	1.515	–	101.1	–	227	–
b3 eq	2.320	2.365	2.742	3.926	1.384	1.818	104.2	105.0	228	214
b4 ax	2.306	2.308	3.528	3.689	1.378	1.827	96.7	110.6	262	232
b4 eq	2.314	2.316	3.431	3.518	1.373	1.837	95.5	101.9	259	235

layer of Au_{13}. Examples of such "irregular" structures are shown in Fig. 6. A common feature of this type of structures is a long C-E distance. These structures may be described as antiprisms, where the six edges on the side are decorated by further Au atoms. The coordination of the central atom Au of the cluster is no longer bulk-like and the average Au coordination is lower than in "regular" structures. This reduced effective Au-Au coordination is reflected by various properties, as will be discussed below. Thus, compared to the compact Au_{13} core of the regular structures, these more open structures may better be considered as complex compounds than as ligated metal clusters.

Structure and stability

For the irregular structures, we distinguish the sites b3 and b4 when bridging S centers of the ligands are tilted toward neighboring three- and fourfold sites, respectively (Fig. 2d). One has to be aware that this labeling gets meaningless when the S atoms of the ligands lie in the plane of equatorial Au atoms (Fig. 5). For $Au_{13}(SH)_6$, we optimized all variants of these types of structures. The only peculiarity observed is a rather short Au-H contact (1.81 Å) in the structure b3 ax (b3 coordination with axial orientation of the SH ligands); on the other hand, this structure exhibits a rather long S-H bond of 1.5 Å. For SMe ligands, no stable structure could be obtained for a b3 ax starting geometry; optimization lead to a species classified as b4 ax.

Pertinent characteristics of ligand bonding in irregular structures are collected in Table 6. Except for structure b3 eq with SMe, the Au-S distances, 2.31 – 2.32 Å, fall in between the values calculated for singly or twofold coordinated ligands in regular structures. This reflects the increased bonding capability of the involved Au atoms which results from their lower effective coordination. Consequently, also S-H bond lengths of 1.38 Å and S-C bond lengths of 1.83 Å are at the upper limit of previously calculated results. As already mentioned, SH in a b3 ax configuration forms an exception. A second exception is the structure b3 eq for SMe, which closely resembles bridge coordinated regular structures. Here the S atoms of the ligand lie nearly in plane with the equatorial Au atoms, thus equatorial and axial ligand orientations are quasi degenerate. Indeed, the cluster core of structure b3 eq is not distorted to an irregular type (see below).

Ligand binding energies of irregular structures vary considerably. Irregular clusters of type b3 exhibit lower binding energies than clusters with b4 structure, which range up to 262 kJ/mol (SH), even slightly exceeding the largest values of 258 kJ/mol found for four bridging SH ligands in regular structures (Table 2, D_{2h} b eq). Comparison of regular and irregular structures with six bridging ligands shows that irregular b3 structures are slightly weaker bound, while the ligand bond strength of b4 structures exceeds that of regular structures by $\sim$ 20 kJ/mol for SH and $\sim$ 15 kJ/mol for SMe (Tables 2 and 6). The characteristics of the metal core of irregular structures (Table 7) confirm the interpretation given above. Except for structure b3 eq with SMe ligands, the average Au-Au distances are calculated at values comparable to (or above of) the nearest-neighbor distance of 2.88 Å for bulk gold [52]. This criterion clearly differentiates these irregular structures from the regular ones. Correspondingly, the average Au-Au coordination, only 3.7, is smaller by almost two units (Table 7). C-A distances are rather short, more than 0.1 Å below the value of the bare cluster, reflecting the considerable weakening of the C-E contacts. These latter distances, calculated at 3.1 – 3.35 Å, clearly exceed those of normal Au-Au bonds. The angles A-C-A still stay close to the reference of 60°. Also the Au related geometric parameters confirm the classification of the structure b3 eq with SMe ligands as regular. In this special case, the Au-Au coordination amounts to 5.5, the average Au-Au distance of 2.78 Å is shorter than for irregular structures, and the distances C-E and C-A are similar, in line with typical results for regular structures (Table 3).

Table 7. Cluster-core related characteristics of irregular structures of $Au_{13}(SR)_6$ in D_{3d} symmetry, R = H, Me: average Au-Au coordination numbers c and distances ⟨d⟩ as well as selected Au-Au bond lengths and angles. Structures are labeled by coordination site (b3 = bridge toward threefold, b4 = bridge towards fourfold) and ligand orientation (ax = axial, eq = equatorial). Bond lengths in Å, angles in degree, and energies in kJ/mol. For the atom labels C, A, and E, see Fig. 1.

Structure	c		⟨d⟩		C-A		C-E		A-C-A	
	H	Me	H	Me	H	Me	H	Me	H	Me
b3 ax	3.69	–	2.965	–	2.677	–	3.227	–	59.3	–
b3 eq	3.69	5.54	2.991	2.776	2.591	2.736	3.347	2.815	63.6	59.6
b4 ax	3.69	3.69	2.910	2.898	2.617	2.604	3.181	3.171	64.0	65.0
b4 eq	3.69	3.69	2.888	2.874	2.623	2.627	3.135	3.105	63.9	63.8

Table 8. Electronic structure of irregular structures of $Au_{13}(SR)_6$, R = H, Me, from LDA calculations: Mulliken charges q per ligand and of the cluster core Au_{13} in *e*, ionization potential IP, and electron affinity EA, and energy ε_{HOMO} of the HOMO in eV. Structures are labeled by coordination site (b3 = bridge toward threefold, b4 = bridge towards fourfold) and ligand orientation (ax = axial, eq = equatorial).

Structure	q(SR)		q(Au_{13})		IP		EA		ε_{HOMO}	
	H	Me	H	Me	H	Me	H	Me	H	Me
b3 ax	−0.22	–	1.32	–	5.66	–	2.59	–	−4.13	–
b3 eq	−0.28	−0.07	1.70	0.43	5.73	5.99	2.69	3.06	−4.21	−4.50
b4 ax	−0.11	−0.09	0.64	0.52	6.20	6.01	3.06	3.01	−4.64	−4.51
b4 eq	−0.15	−0.10	0.88	0.60	5.90	5.47	2.78	2.51	−4.34	−3.99

Electronic structure

In comparison to regular structures, SH ligands at the b3 site are somewhat more negatively charged, whereas all other cases yield rather low values (Table 8). Consequently, also the positive charge of the Au_{13} moiety is larger for the SH b3 configuration then for the regular D_{3d} structures, but lower for the other irregular configurations. As for the regular structures, the charge separation is smaller for SMe than for SH ligands. In line with a tendency to higher lying HOMO levels, also IP and EA values of the irregular structures are lower than for the more compact regular structures (Table 8). The DOS of the irregular species shows an Au(sp) dominated peak at the Fermi energy which is separated by a gap from the Au(d) dominated rest of the valence DOS, not present for regular structures. These general trends again corroborate the separation of species examined into sets with regular and irregular structures.

Conclusions

All-electron scalar relativistic density functional calculations have been performed to study the effect of SH and SMe ligands on the model cluster Au_{13}, while various symmetry constraints were imposed on the cluster. Different ligand coordinations have been inspected for four, six, and eight ligands, where the largest coverage is comparable to estimates for experimentally studied larger gold thiolate clusters. In this way, we carried out for the first time a detailed comparison of structural as well as electronic features of gold thiolate clusters with a rather accurate method, thus providing information on how the properties of such species vary with ligand coverage and coordination mode.

For all cases inspected, twofold coordination of thiolate ligands has been preferred. No structures were found with ligands at sites with higher metal coordination. However, the energetic difference between top (175 – 200 kJ/mol for SMe) and bridging coordination (210 – 240 kJ/mol for SMe) as well as the flexibility of the gold cluster core does not allow one to exclude definitely three- or fourfold sites, especially when thiolates with larger substituents are considered where ligand-ligand interaction comes into play.

In most cases considered, the internal coordination as well as the structure of the Au_{13} core is stable under ligand coordination. On the other hand, more open structures have been obtained for six ligands in D_{3d} symmetry, where some of the Au-Au bonds are considerably weakened and elongated beyond the nearest-neighbor distance of bulk gold. These results as well as the rather strong variation of the Au-Au distances illustrate the rather flexible nature of the Au cluster structure. Because the binding energy per Au atom in Au_{13} (194 kJ/mol) is weaker than the gold-ligand interaction, the suggestion of even more stable disordered structures of gold thiolate clusters [18] seems plausible.

With increasing number of ligands, only moderate effects have been obtained for structures with bridging coordination, *e.g.*, a slight reduction of the ligand binding energy (by less than 20 kJ/mol), an elongation of the average Au-Au distance (by 0.05 Å), as well as a tendency to smaller IP and EA values. No clear trends result for top-coordinated ligands. Due to the weak electron donating character of the methyl group, SMe ligands were found to bind weaker than the simple model ligand SH. Also the amount of charge drawn per ligand from the metal core of the cluster is slightly lower for SMe. While the charge of the Au_{13} cluster core increased with increasing number of ligands, the charge per ligand showed no definite trend. The charge separation between metal core and ligand shell is small, less than 1.5 *e* for the largest coverage of methylthiolates. Especially for bridging ligands, IP and EA values are considerably reduced due to ligand coordination.

Because the differences between clusters with SH and SMe ligands are rather uniform, SH may well serve as a reliable model ligand in computational studies of larger species, provided the interpretation of results takes into account the differences discussed here.

Although the model clusters of this study were subjected to symmetry constraints, the resulting structural variations admit the conclusion that gold thiolate clusters are rather flexible species, even at small size. Thus, more elaborate studies probably will reveal an even wider range of ligand coordination geometries and cluster structures.

Acknowledgments

We would like to dedicate this work to H. Schmidbaur on the occasion of his 70th birthday. His beautiful work on carbon-centered Au_6 clusters, dating back to 1988, provided strong motivation to develop an efficient Kohn-Sham procedure for heavy-element compounds. Ultimately, this lead to the efficient scalar relativistic variant of the LCGTO-FF-DF method, also used in the present study, see Ref. [30]. The present work was supported by Deutsche Forschungsgemeinschaft and Fonds der Chemischen Industrie.

[1] M. Brust, M. Walker, D. Bethel, D. J. Schiffrin, R. Whyman, J. Chem. Soc. Chem. Commun. 801 (1994).
[2] A. C. Templeton, W. P. Wuelfing, R. W. Murray, Acc. Chem. Res. **33**, 27 (2000).
[3] M.-C. Daniel, D. Astruc, Chem. Rev. **104**, 293 (2004).
[4] D. Zanchet, C. M. Micheel, W. J. Parak, D. Gerion, S. C. Williams, A. P. Alivisatos, J. Phys. Chem. B **106**, 11758 (2002).
[5] C. M. Niemeyer, B. Ceyhan, P. Hazarika, Angew. Chem. Int. Ed. **42**, 5766 (2003).
[6] C. N. R. Rao, G. U. Kulkarni, P. J. Thomas, P. P. Edwards, Chem. Soc. Rev. **29**, 27 (2000).
[7] M. Brust, C. J. Kiely, Coll. Surf. A **202**, 175 (2002).
[8] J. A. Larsson, M. Nolan, J. C. Greer, J. Phys. Chem. B **106**, 5931 (2002).
[9] W. Andreoni, A. Curioni, H. Grönbeck, Int. J. Quantum Chem. **80**, 598 (2000).
[10] W. D. Luedtke, U. Landman, J. Phys. Chem. **100**, 13323 (1996).
[11] H. Häkkinen, R. Barnett, U. Landman, Phys. Rev. Lett. **82**, 3264 (1999).
[12] S. Letardi, F. Cleri, J. Chem. Phys. **120**, 10062 (2004).
[13] H. Basch, M. A. Ratner, J. Chem. Phys. **119**, 11926 (2003).
[14] D. Krüger, H. Fuchs, R. Rousseau, M. Parrinello, J. Chem. Phys. **115**, 4776 (2001).
[15] I. L. Garzón, K. Michaelian, M. R. Beltrán, A. Posada-Amarillas, P. Ordejón, E. Artacho, D. Sánchez-Portal, J. M. Soler, Phys. Rev. Lett. **81** 1600 (1998).
[16] J. Oviedo, R. E. Palmer, J. Chem. Phys. **117**, 9548 (2002).
[17] J. Wang, G. Wang, J. Zhao, Phys. Rev. B **66**, 035418 (2002).
[18] I. L. Garzón, C. Rovira, K. Michaelian, M. R. Beltrán, P. Ordejón, J. Junquera, D. Sánchez-Portal, E. Artacho, J. M. Soler, Phys. Rev. Lett. **85**, 5250 (2000).
[19] A. Ullman, Chem. Rev. **96**, 1533 (1996).
[20] H. Kondoh, M. Iwasaki, T. Shimada, K. Amemiya, T. Yokoyama, T. Ohta, Phys. Rev. Lett. **90**, 066102 (2003).
[21] M. G. Roper, M. P. Skegg, C. J. Fisher, J. J. Lee, V. R. Dhanak, D. P. Woodruff, R. G. Jones, Chem. Phys. Lett. **389**, 87 (2004).
[22] H. S. Kato, J. Noh, M. Hara, M. Kawai, J. Phys. Chem. B **106**, 9655 (2002).
[23] F. Schreiber, J. Phys. Cond. Mat. **16**, R881 (2004) and references therein.
[24] H. Grönbeck, A. Curioni, W. Andreoni, J. Am. Chem. Soc. **122**, 3839 (2000).
[25] Y. Akinaga, T. Nakajima, K. Hirao, J. Chem. Phys. **114**, 8555 (2001).
[26] Y. Morikawa, T. Hayashi, C. C. Liew, H. Nozoye, Surf. Sci. **507-510**, 46 (2002).
[27] B. I. Dunlap, N. Rösch, Adv. Quantum Chem. **21**, 317 (1990).
[28] Th. Belling, T. Grauschopf, S. Krüger, M. Mayer, F. Nörtemann, M. Staufer, C. Zenger, N. Rösch, in H.-J. Bungartz, F. Durst, C. Zenger (eds): High Performance Scientific and Engineering Computing, Proceedings of

the First International FORTWIHR Conference 1998, Lecture Notes in Computational Science and Engineering, Vol. 8, p. 439 – 453, Springer, Heidelberg (1999).
[29] Th. Belling, T. Grauschopf, S. Krüger, F. Nörtemann, M. Staufer, M. Mayer, V. A. Nasluzov, U. Birkenheuer, A. Shor, A. Matveev, A. Hu, M. S. K. Fuchs-Rohr, K. M. Neyman, D. I. Ganyushin, T. Kerdcharoen, A. Woiterski, N. Rösch, PARAGAUSS, Version 2.2, Technische Universität München (2001).
[30] O. D. Häberlen, N. Rösch, Chem. Phys. Lett. **199**, 491 (1992).
[31] N. Rösch, S. Krüger, M. Mayer, V. A. Nasluzov, in J. Seminario (ed): Theoretical and Computational Chemistry, Vol. 4, Recent Developments and Applications of Modern Density Functional Theory, p. 497, Elsevier, Amsterdam (1996).
[32] N. Rösch, A. V. Matveev, V. A. Nasluzov, K. M. Neyman, L. Moskaleva, S. Krüger, in P. Schwerdtfeger (ed): Relativistic Electronic Structure Theory – Applications, Theoretical and Computational Chemistry Series, p. 656, Elsevier, Amsterdam (2004).
[33] S. Vosko, L. Wilk, M. Nusair, Can. J. Phys. **58**, 1200 (1980).
[34] A. D. Becke, Phys. Rev. A **38**, 3098 (1988).
[35] J. P. Perdew, Phys Rev B **33**, 8822 (1986); J. P. Perdew, Phys Rev B **34**, 7406 (1986).
[36] S. Krüger, M. Stener, N. Rösch, J. Chem. Phys. **114**, 5207 (2001).
[37] V. A. Nasluzov, N. Rösch, Chem. Phys. **210**, 413 (1996).
[38] O. D. Häberlen, S.-C. Chung, N. Rösch, Int. J. Quantum Chem. **106**, 5189 (1997).
[39] A. Görling, S. B. Trickey, P. Gisdakis, N. Rösch, in Topics in J. Brown, P. Hofmann (eds): Organometallic Chemistry, Vol. 4, p. 109, Springer, Heidelberg (1999).
[40] A. D. Becke, J. Chem. Phys. **88**, 2547 (1988).
[41] V. I. Lebedev, Zh. Vychisl. Mat. Mat. Fiz. **16**, 293 (1976).
[42] Au: O. D. Häberlen, S.-C. Chung, N. Rösch, Int. J. Quantum. Chem., Quantum Chem. Symp. **28**, 595 (1994); H: s-exponents from F. B. Van Duijneveldt, IBM Res. Rep. RJ 945 (1971); p-exponent (1.0) from M. J. Frisch, J. A. Pople, J. S. Binkley, J. Chem. Phys. **80**, 3265 (1984); S: A. Veillard, Theor. Chim. Acta **12**, 405 (1968); C: O. D. Häberlen, N. Rösch, J. Phys. Chem. **97**, 4970 (1993).
[43] L. D. Marks, Rep. Prog. Phys. **57**, 603 (1994).
[44] C. L. Cleveland, U. Landman, T. G. Schaaff, M. N. Shafigullin, P. W. Stephens, R. L. Whetten, Phys. Rev. Lett. **79**, 1873 (1997).
[45] G. Schmid, in G. Schmid (ed): Clusters and Colloids, p. 178, VCH, Weinheim (1994).
[46] T. Schaaff, M. Shafigullin, J. Khoury, I. Wezmar, R. L. Whetten, J. Phys. Chem. B **105**, 8785 (2001).
[47] G. Schmid, Inorg. Synth. **27**, 214 (1990).
[48] R. L. Whetten, J. T. Khoury, M. M. Alvarez, S. Murthy, I. Vezmar, Z. L. Wang, P. W. Stephens, C. L. Cleveland, W. D. Luedtke, U. Landman, Adv. Mater. **8**, 428 (1996).
[49] O. D. Häberlen, S.-C. Chung, M. Stener, N. Rösch, J. Chem. Phys. **106**, 5189 (1997).
[50] S. Krüger, S. Vent, N. Rösch, Ber. Bunsenges. Phys. Chem. **101**, 1640 (1997).
[51] N. S. Phala, G. Klatt, E. van Stehen, Chem. Phys. Lett. **395**, 33 (2004).
[52] R. C. Weast (ed), CRC Handbook of Chemistry and Physics, 64 ed., CRC Press, Boca Raton (1983).
[53] S. Krüger, S. Vent, F. Nörtemann, M. Staufer, N. Rösch, J. Chem. Phys. **115**, 2082 (2001).
[54] S. Krüger, M. Stener, M. Mayer, F. Nörtemann, N. Rösch, J. Mol. Struct. (Theochem) **527**, 63 (2000).
[55] A. Woiterski, S. Krüger, A. M. Shor, A. Genest, N. Rösch, to be published.
[56] T. G. Schaaff, G. Knight, M. N. Shafigullin, R. F. Borkman, R. L. Whetten, J. Phys. Chem. B **102**, 10643 (1998).
[57] R. L. Donkers, D. Lee, R. W. Murray, Langmiur **20**, 1945 (2004).
[58] I. L. Garzón, E. Artacho, M. R. Beltrán, A. García, J. Junquera, K. Michaelian, P. Ordejón, C. Rovira, D. Sánchez-Portal, J. M. Soler, Nanotechnology **12**, 126 (2001).
[59] L. H. Dubois, R. G. Nuzzo, Ann. Phys. Chem. **43**, 437 (1992).